Compartmentalization of superoxide dismutase 1 (SOD1G93A) aggregates determines their toxicity

Sarah J. Weisberg[a,1], Roman Lyakhovetsky[b,1], Ayelet-chen Werdiger[b], Aaron D. Gitler[c], Yoav Soen[a], and Daniel Kaganovich[b,2]

[a]Department of Biological Chemistry, Weizmann Institute of Science, Rehovot 76100, Israel; [b]Department of Cell and Developmental Biology, Alexander Silberman Institute of Life Sciences, Hebrew University of Jerusalem, Jerusalem 91904, Israel; and [c]Department of Genetics, Stanford University School of Medicine, Stanford, CA 94305

Edited by Gregory A. Petsko, Brandeis University, Waltham, MA, and approved August 17, 2012 (received for review April 5, 2012)

Neurodegenerative diseases constitute a class of illnesses marked by pathological protein aggregation in the brains of affected individuals. Although these disorders are invariably characterized by the degeneration of highly specific subpopulations of neurons, protein aggregation occurs in all cells, which indicates that toxicity arises only in particular cell biological contexts. Aggregation-associated disorders are unified by a common cell biological feature: the deposition of the culprit proteins in inclusion bodies. The precise function of these inclusions remains unclear. The starting point for uncovering the origins of disease pathology must therefore be a thorough understanding of the general cell biological function of inclusions and their potential role in modulating the consequences of aggregation. Here, we show that in human cells certain aggregate inclusions are active compartments. We find that toxic aggregates localize to one of these compartments, the juxtanuclear quality control compartment (JUNQ), and interfere with its quality control function. The accumulation of SOD1G93A aggregates sequesters Hsp70, preventing the delivery of misfolded proteins to the proteasome. Preventing the accumulation of SOD1G93A in the JUNQ by enhancing its sequestration in an insoluble inclusion reduces the harmful effects of aggregation on cell viability.

aggregation quality control | ALS | insoluble protein deposit | protein folding

Because of the propensity of incorrectly folded proteins to aggregate, the misfolding of a protein represents an existential threat to the cell and has driven the evolution of an elaborate quality control system. A specialized machinery of chaperones bind nonnative polypeptides and promote their folding (1, 2), or target them for degradation by the ubiquitin–proteasome system (3). The threat of toxic protein aggregation extends to the entire organism in the form of diseases (4) brought on by the failure of certain cells to properly manage proteins that have lost their native structure because of mutations, aging, or stress (5, 6).

Neurodegenerative diseases, including amyotrophic lateral sclerosis (ALS), Parkinson disease, Alzheimer's disease, and polyglutamine expansion diseases, are a class of illnesses marked by the progressive degeneration of specific subpopulations of neurons. The neuronal damage observed in these maladies has been linked to pathological protein aggregation. The disease phenotype is characterized by the formation of intracellular or extracellular plaques or inclusions containing amyloid forms of the disease-causing proteins. Despite this commonality, most neurodegenerative disease-related proteins, whose biochemical features have been extensively analyzed in systems in vivo and in vitro, do not share primary sequence features, or functional characteristics, but do aggregate into amyloid superstructures in a generally similar fashion (4, 7–9). Given the pronounced association of amyloid formation with disease, a long-standing hypothesis assumed that amyloid inclusions were the culprits of pathology. Several recent studies have surprisingly observed that the insoluble aggregate deposits are themselves not the main source of toxicity (10–13) and may even be protective. This new model suggests that active aggregation is a mechanism used by cells to remove harmful aggregates from the cytosolic milieu (11, 14).

When the protein folding balance tends toward misfolding and aggregation, aberrant proteins accumulate in cell biologically distinct inclusion structures, which had once been assumed to form as a passive consequence of insoluble protein deposition. Recent findings suggest that the appearance of inclusions, rather than being a failure of the quality control process, represent the continuation of quality control by other means. Inclusions have been implicated in the task of disaggregating, degrading, or sequestering harmful aggregated proteins (15–18). Moreover, since inclusions can appear in any cell type in different organisms it is likely that they have a homeostatic role in the cellular response to misfolding and aggregation. The question of whether inclusions are a response to toxicity or are themselves toxic has, however, been a point of controversy.

In yeast, misfolded proteins first aggregate in small cytosolic stress foci, and then are partitioned to two distinct compartments, the juxtanuclear quality control compartment (JUNQ) and the insoluble protein deposit (IPOD) (15). The JUNQ contains ubiquitinated proteins marked for proteasomal degradation. The IPOD contains insoluble aggregates, amyloidogenic proteins, and chaperones such as Hsp104 (15). Targeting a soluble misfolded protein to the IPOD instead of the JUNQ can alter its solubility properties by inducing its formation into an insoluble aggregate structure.

Here, we present direct evidence of a quality control function for JUNQ inclusions in human cultured cells. JUNQ compartments concentrate soluble misfolded proteins together with chaperones and proteasomes, and facilitate their degradation. Our data show that the accumulation of insoluble aggregates in the JUNQ inhibits the degradation of other misfolded proteins by sequestering the essential chaperone Hsp70 and thereby blocking the path of quality control substrates to the proteasome. Remarkably, rerouting toxic aggregates from the JUNQ to an insoluble polyQ inclusion restores the JUNQ protein degradation function and rescues cell viability. We show that toxic and nontoxic inclusions represent different sites of aggregate deposition, with different cell biological properties. Our data define a potentially broadly applicable context for designing interventions for neurodegenerative diseases associated with protein misfolding.

Results

Mammalian Cells Localize Aggregates to Distinct Inclusions. Previous work has described a mechanism through which the cellular quality control network distinguishes between two classes of aggregation-prone proteins: soluble or "normal" misfolded proteins and amyloidogenic proteins (Fig. 1*A*) (15). Normal misfolded proteins arise as a result of mutations or stress-induced damage (such as in the case of Luciferase or Ubc9^{ts}), or when

Author contributions: S.J.W., Y.S., and D.K. designed research; S.J.W., R.L., A.-c.W., A.D.G., and D.K. performed research; A.D.G. and Y.S. contributed new reagents/analytic tools; S.J.W., A.D.G., and D.K. analyzed data; and S.J.W. and D.K. wrote the paper.

The authors declare no conflict of interest.

This article is a PNAS Direct Submission.

Freely available online through the PNAS open access option.

[1]S.J.W. and R.L. contributed equally to this work.

[2]To whom correspondence should be addressed. E-mail: dan@cc.huji.ac.il.

This article contains supporting information online at www.pnas.org/lookup/suppl/doi:10.1073/pnas.1205829109/-/DCSupplemental.

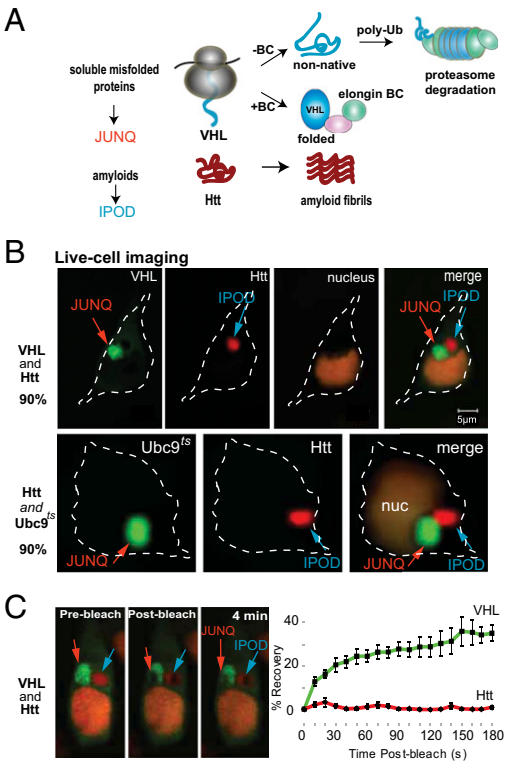

Fig. 1. Aggregates localize to distinct inclusion sites in mammalian cells. (*A*) VHL and polyQ Htt are models for two types of aggregation-prone proteins. Soluble misfolded proteins accumulate in the JUNQ, whereas amyloidogenic proteins are sequestered in an IPOD-like inclusion. (*B*) Inclusions were visualized by expression of VHL-GFP and HttQ97-mRFP, respectively; nuclei in all experiments were visualized with NLS-TFP. One-micrometer confocal slices are shown in all panels, and percentage observed phenotype is indicated on the left side of the images. (*C*) FRAP experiments reveal different mobility properties of VHL in the JUNQ vs. Htt. An area within the inclusion was bleached with full laser power for 2 s. Images represent inclusion fluorescence before, immediately after, and 4 min after bleach (*Left* to *Right*). Graphs are average recovery over time from five experiments. Error bars represent standard error.

a folding-incompetent protein is expressed as an unassembled subunit [such as in the case of Von Hippel–Lindau (VHL)] (6). In yeast, these normal misfolded proteins form soluble aggregates and are targeted to the JUNQ where they colocalize with quality control machinery. Amyloidogenic proteins [such as polyQ Huntingtin (Htt) and certain yeast prionogenic proteins such as Rnq1 and Ure2] constitutively form insoluble aggregates and are sent to the IPOD (15).

Given that yeast studies of JUNQ and IPOD (15) as well as several studies in mammalian cells (19) have observed aggregate inclusions with different properties, we set out to coexpress different types of aggregation-prone proteins to track their localization and effect on cell viability. By imaging live cells expressing fluorescently tagged proteins, we observed that in human cells, as in yeast, normal misfolded proteins (VHL and Ubc9^{ts}) localize to JUNQ-like compartments (Fig. 1*B*). JUNQs demonstrated a dependence of formation on cellular transport, implying the existence of active delivery mechanisms regulated by the quality control system (15–17). JUNQs were also localized near the microtubule-organizing center (MTOC) (Fig. 1*B*). Htt, on the other hand, is sequestered in a spatially distinct inclusion (Fig. 1*B*). VHL forms JUNQ inclusions in most cells (~70%; cells that are expressing a high level of the protein) without proteasome inhibition, whereas mild proteasome inhibition leads to the formation of inclusions in all cells. Consistent with previous findings in yeast, simultaneous two-color fluorescence recovery after photobleaching (FRAP) experiments showed that proteins in the mammalian JUNQ have a ~40% mobile fraction (Fig. 1*C*). Htt, on the other hand, is completely immobile and is fully sequestered from the cytosol (Fig. 1*C*).

Other studies in mammalian cells have characterized several types of aggregate inclusion bodies (IBs). Until now, nearly all IBs in mammalian cells were called aggresomes, of which there was thought to be one per cell and which were characterized by perinuclear localization, and the dependence on microtubules for formation. It has recently been observed, however, that some typical "aggresome substrates" such as polyQ Htt actually localize to inclusions in a microtubule-independent manner and are often observed some distance from the MTOC (20). We suggest that this contradiction can be resolved by differentiating between different types of IBs. We therefore refer to juxtanuclear inclusions with mobile quality control substrates as JUNQs, and the polyQ Htt inclusions as IPODs, to distinguish between these distinct types of inclusion phenotypes.

Localization of Poorly Soluble Aggregates to the JUNQ Leads to Toxicity. Although any cellular protein can become misfolded, and many proteins do misfold under normal conditions (4, 21), only a handful of misfolded proteins have been implicated in disease pathologies characterized by IB formation. Two critical questions are, therefore, (*i*) what determines the toxicity of certain aggregates, and (*ii*) what role IBs play in toxicity. Conflicting models exist for the relationship between IB formation and cell viability. In particular, there is evidence that the accumulation of Htt in an IB is protective of cell viability (10, 13), whereas cytosolic Htt that fails to be sequestered in an IB is more toxic (22). Other experiments have suggested that familial ALS (fALS)-associated mutant SOD1 is most toxic when localized to an IB (8). It has also been shown that toxic SOD1 IBs are more dynamic than Htt inclusions, and interact with quality control machinery (19, 23). The

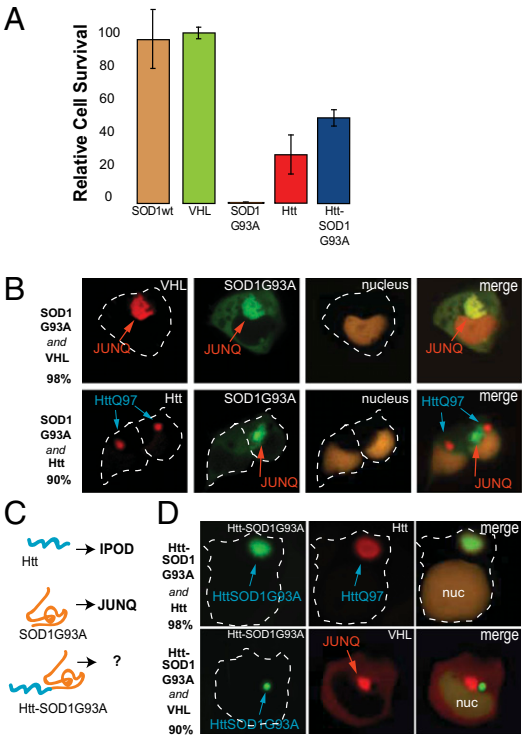

Fig. 2. Aggregate toxicity accompanies localization of G93A to the JUNQ. (*A*) Twenty-four hours posttransfection, cells were sorted according to fluorescent protein expression level, allowed to recover, and monitored for viability using an MTS assay. Htt-SOD1G93A is significantly less toxic than G93A. (*B*) G93A inclusions are JUNQs. G93A colocalizes with VHL but not with Htt. (*C*) A fusion protein of Htt-SOD1G93A-YFP. (*D*) Htt-SOD1G93A colocalizes exclusively with Htt (*Upper*) and is absent from the JUNQ (*Lower*).

differences between these IBs may represent differences in function (degradation vs. sequestration). We therefore reasoned that the disparate outcomes of mutant SOD1 and Htt IB formation could reflect differences in localization relative to the JUNQ. In other words, the toxicity of aggregates might depend on whether they are allowed to accumulate in a compartment that carries out an essential folding or degradation function, or an IB that only sequesters aggregates.

To test the idea that toxic and protective inclusions are different cellular compartments, we first compared the effects of ectopically expressing ALS-associated SOD1 G93A (G93A), polyQ Htt, a normal misfolded protein (VHL), and wild-type SOD1 (all tagged with GFP) on cell viability (Fig. 2*A*). Cell populations from each sample with similar fluorescence intensity were sorted by FACS, and assayed for cell viability using a 3-(4,5-dimethylthiazol-2-yl)-5-(3-carboxymethoxyphenyl)-2-(4-sulfophenyl)-2*H*-tetrazolium (MTS) kit. G93A was indeed more toxic than the Htt or nontoxic controls. Cell viability was assayed at a time post-transfection when most G93A- and Htt-expressing cells formed IBs. We therefore asked whether G93A localized to the JUNQ. G93A did not coaggregate with Htt but was observed exclusively in the JUNQ, together with VHL and quality control factors (Fig. 2*B*). Localization of a misfolded protein to the JUNQ was not by itself sufficient to induce toxicity because VHL-expressing cells were healthy despite most cells forming JUNQ inclusions (Fig. 2*A*).

We posited that if aggregation toxicity is caused by the localization of G93A in the JUNQ, then it stands to reason that the toxicity could be reversed if the toxic aggregates were sequestered in the Htt IB. We therefore fused G93A to Htt (Fig. 2*C*), hypothesizing that the stretch of 97 glutamines would facilitate rapid polymerization of Htt-SOD1G93A into an amyloid, thus preventing it from entering the JUNQ. Strikingly, the Htt-SOD1G93A fusion protein was now completely relocalized to the Htt inclusion (Fig. 2*D*). More importantly, confining G93A to the Htt IB alleviated much of its toxic effect (Fig. 2*A*). Thus, localization is a major determinant of whether an aggregate is toxic. Moreover, modulating subcellular location determines the physiological impact of aggregation.

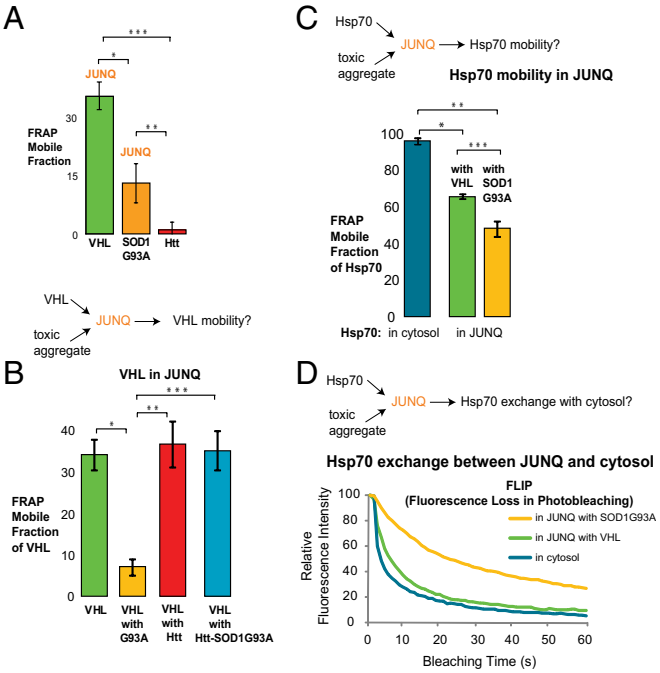

Fig. 4. G93A aggregates reduce VHL and Hsp70 mobility in the JUNQ. (*A*) FRAP ($n = 10$) reveals that toxic proteins in the JUNQ are less mobile than nontoxic JUNQ substrates. Recovery of G93A in JUNQ was higher than of Htt, but lower than that of VHL. $*P \leq 0.0019$; $**P \leq 0.0248$; $***P \leq 0.0044$. (*B*) Toxic proteins in JUNQ decrease the mobility of VHL. JUNQ inclusions containing VHL were analyzed by FRAP in the presence of G93A. Htt is localized to the IPOD and thus has no effect on VHL mobility in the JUNQ. Htt-SOD1G93A does not have any effect on VHL mobility in the JUNQ. $*P \leq 0.001$; $**P \leq 0.0067$; $***P \leq 0.0017$. (*C*) G93A aggregates impair the mobility of Hsp70 in the JUNQ. $*P \leq 0.0001$; $**P \leq 0.0002$; $***P \leq 0.024$. (*D*) G93A in the JUNQ leads to sequestration of Hsp70. Exchange of Hsp70 between the cytosol and the JUNQ decreased when G93A but not VHL accumulated there.

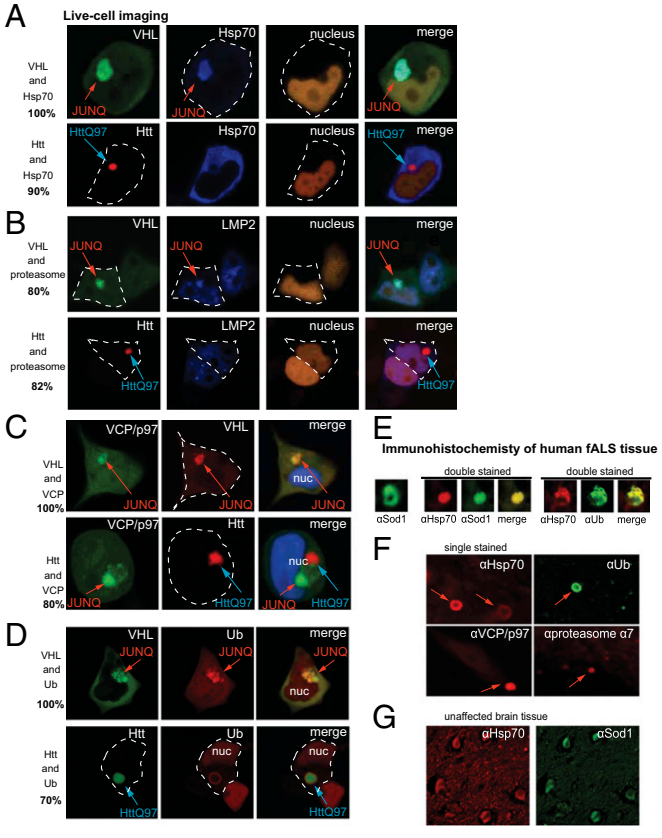

Fig. 3. The JUNQ is a site of cellular quality control. (*A*) Hsp70-YFP localizes to the JUNQ but not the Htt inclusion. (*B*) An enrichment of the proteasome is seen in the JUNQ but not in the Htt inclusion. Proteasomes were visualized with LMP2-YFP. (*C*) p97 colocalizes with VHL in JUNQ but not with Htt. (*D*) Ubiquitin colocalizes with VHL in the JUNQ. (*E*) Immunohistochemical analysis of spinal cord sections from an fALS patient harboring a mutation in SOD1(D124V) reveals motor neurons containing inclusions that costain with SOD1 and Hsp70 (*Left*), and for ubiquitin and Hsp70 (*Right*). Single staining is shown in *F* and control (non-ALS) spinal cord sections in *G*.

JUNQ Is a Cellular Quality Control Site. Having observed the marked improvement of cell viability as a result of preventing G93A from aggregating in the JUNQ, we sought a mechanistic explanation for why G93A aggregation in the JUNQ is toxic. First, we characterized the quality control function of the mammalian JUNQ inclusion. Immunofluorescence analysis showed that essential quality control factors reside in the JUNQ (Fig. S2*A*). We used live-cell imaging for subsequent experiments to visualize delicate and transient structures and to ensure that the compartments that we were imaging were indeed JUNQs by virtue of their morphology and mobility properties. Proteasomes, p97, ubiquitin, and the stress-induced Hsp70 chaperone colocalized with VHL in the JUNQ (Fig. 3 *A–D* and Fig. S2*B*) but were absent from the Htt IB (Fig. 3 *A* and *B*). In some cases, ubiquitinated and misfolded proteins form a submicrometer ring around the Htt IB, arguably because a large exposed surface of polyQ adsorbs poorly folded proteins (24). Htt IBs were also strongly encircled by a dynamic ring of yeast Hsp104 expressed in human cells as reported previously (24) (Fig. S2*B*).

fALS Spinal Cord Neurons Contain Hsp70- and Ubiquitin-Positive Inclusions. Given the well-established association of SOD1 aggregation with disease pathology, our cell biological G93A aggregation model provided an opportunity to probe the correlation between our basic model and disease phenomena. Brain and spinal cord tissue from patients with fALS caused by different SOD1 mutations has previously been shown to contain ubiquitin-positive and SOD1-positive IBs (26). To establish a preliminary connection between the characterization of the G93A JUNQ and similar IBs observed in fALS patients, we analyzed sections of cervical spinal cord and medulla from an individual who was diagnosed with ALS at age 58 and died at age 63. This individual was found to harbor a heterozygous mutation in the *SOD1* gene, predicted to result in a D124V substitution. This substitution has previously been shown to be pathogenic (26). We stained these sections with JUNQ markers (Hsp70, ubiquitin, proteasome, and p97). fALS tissue contained IBs that stained positively for these markers, suggesting that the IBs we observe in cell culture may be similar to those seen in mutant SOD1-expressing patients (Fig. 3*F*). We performed double-staining experiments to determine whether SOD1, ubiquitin, and Hsp70 all localized to the same IBs. Indeed, Hsp70- and ubiquitin-positive IBs costained with SOD1 (Fig. 3*E*), whereas spinal cord tissue from three independent healthy controls did not have Hsp70-positive IBs (Fig. 3*G*). These data link our cell biological model to the substantial previous work demonstrating that ubiquitin and SOD1-positive IBs are the hallmark of some SOD1 mutation–associated fALS cases. It should be noted that, in our study, the aggregating proteins are expressed severalfold over endogenous levels, and that this may dictate the cellular response that we observe. Because similar IBs appear in human pathology sections, in future research it will be critical to assess the extent to which the cell biology of motor neurons can be modeled in culture.

G93A Aggregates Disrupt the Mobility of VHL and Hsp70 in the JUNQ. Aggregates have been proposed to cause cytotoxicity by diminishing the capacity of the protein folding machinery (21). The apparent role of the JUNQ in quality control led us to posit that immobile aggregates, if localized in the JUNQ, could absorb cellular quality control resources. We reasoned that the quality control function of the JUNQ would depend heavily on free mobility of the substrates and factors therein. Hence, mobility of normal JUNQ substrates, such as VHL, can serve as a reporter of its healthy function. FRAP experiments revealed that JUNQ-localized G93A, on the other hand, exhibited substantially less mobility than normal misfolded proteins (Fig. 4*A*). Suspecting that G93A might affect quality control in the JUNQ, we tested the effect of having these toxic proteins in the JUNQ on the mobility of VHL. As predicted, VHL showed substantially lower mobility when colocalizing in the JUNQ with G93A than when expressed alone or with Htt (Fig. 4*B*). Similarly, we observed that coexpression with G93A, but not Htt, increased the whole-cell Sarkosyl-insoluble pool of VHL (Fig. S1*A*). Removing G93A from the JUNQ restored VHL mobility (Fig. 4*B*).

Previous work has shown that the folding and degradation of VHL and other misfolded proteins requires Hsp70 (6, 27). Under normal conditions, Hsp70 exchanges freely between the JUNQ and the cytosol (Fig. 4 *C* and *D*). Hence, we examined the diffusion of Hsp70 in JUNQs containing a toxic aggregate. When G93A was localized in the JUNQ, it impeded the mobility of Hsp70 in the JUNQ, and even more severely impaired Hsp70 exchange between the JUNQ and the cytosol (Fig. 4*D*).

G93A Aggregates Inhibit the Degradation of VHL in the JUNQ. To gain insight into the mechanism by which toxic aggregates in the JUNQ influence function, we examined their effect on the degradation of a quality control substrate (VHL) and a natively folded proteasome substrate (Ub-R-YFP) (28). When we monitored steady-state levels of VHL and Ub-R-YFP by FACS, we observed that G93A (but not Htt) inhibited VHL degradation (Fig. 5 *A* and *B*). G93A inhibited VHL degradation to the same extent as the proteasome inhibitor. G93A did not, however, inhibit the degradation of Ub-R-YFP (Fig. 5*B*). This indicates that the toxic aggregate affected the degradation of misfolded proteins only, inhibiting a process upstream of the proteasome. Although both VHL and Ub-R-YFP were degraded by the

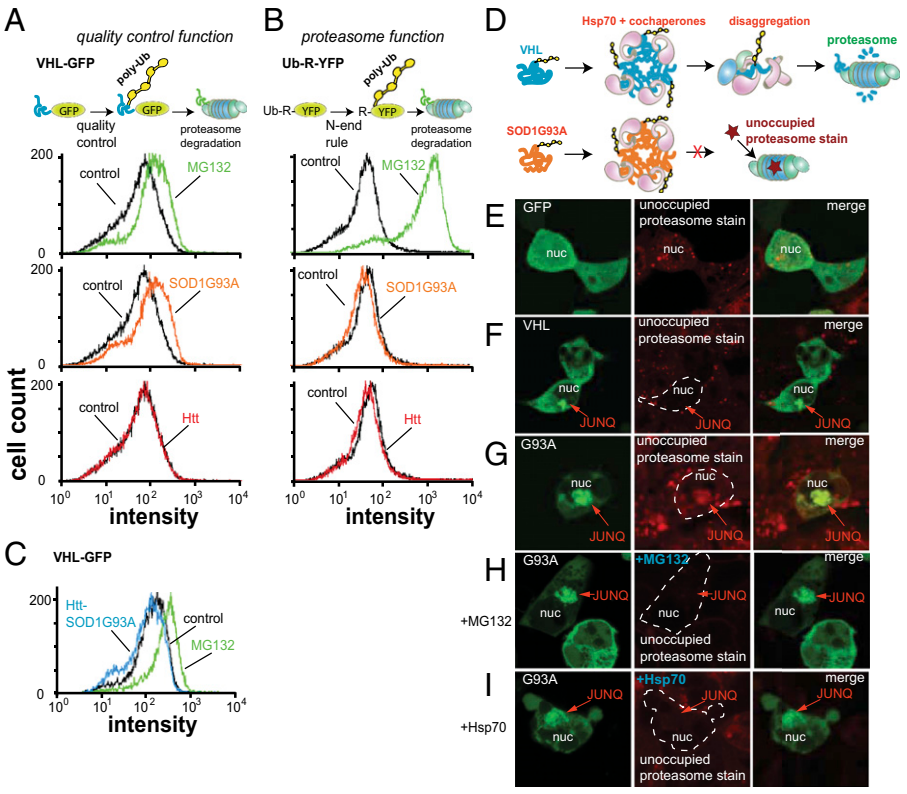

Fig. 5. G93A inhibits degradation of quality control substrates in the JUNQ. (*A*) G93A in the JUNQ but not Htt aggregated separately inhibit the degradation of VHL. Cells stably expressing VHL-GFP were transfected with G93A-CFP or Htt-mRFP, and GFP fluorescence was quantified by FACS. Cells were treated with proteasome inhibitor (2 μM MG132) for 6 h. (*B*) Neither G93A nor Htt directly inhibit the proteasome. Fluorescence levels in cells stably expressing Ub-R-YFP were analyzed as above. (*C*) Unlike G93A, Htt-SOD1G93A does not inhibit VHL degradation. (*D*) Model of proteasome function in the JUNQ. When toxic aggregates sequester Hsp70, quality control substrates fail to be delivered to JUNQ proteasomes, which are then stained by MVB151. (*E*) GFP-expressing cells show diffuse MVB151 staining. (*F*) VHL JUNQs inclusions do not stain with MVB151. (*G*) G93A JUNQs are stained with MVB151. (*H*) MVB151 staining of G93A JUNQs is prevented by washing with MG132. (*I*) Toxic JUNQ MVB151 staining is also abolished by Hsp70, which allows for substrate delivery to proteasomes.

proteasome, VHL and many other quality control substrates have been shown to require additional quality control factors such as Hsp70 to be degraded (6). Given that G93A in the JUNQ reduces Hsp70 mobility (Fig. 4 *C* and *D*), we suspected that G93A inhibits VHL degradation by reducing the functional pool of Hsp70 and other factors, but not by directly inhibiting the proteasome. Indeed, none of the aggregates that we tested caused proteasome inhibition (Fig. 5 *A* and *B*).

To confirm this hypothesis, we observed cells with a nontoxic VHL JUNQ and cells with a toxic G93A JUNQ and stained with a fluorescent proteasome probe [MVB151 (29)]. This probe is a derivative of the proteasome inhibitor MG132. When MVB151 is able to enter a functional proteasome, it binds irreversibly and therefore tags it fluorescently, even after washout of the probe (Fig. 5 *D* and *E*). Proteasomes that are active but occupied by MG132 are not marked by MVB151 (29). VHL JUNQs were not stained with MVB151 (although there was diffuse cytosolic staining), indicating that the proteasomes that localize in these inclusions (Fig. 3*B*) are actively degrading substrate (Fig. 5*F*). As predicted by our model, however, G93A JUNQs showed strong MVB151 staining, suggesting that proteasomes in these inclusions are more likely to be unoccupied but still functional (Fig. 5*G*) [hence prewashing the cells with MG132 abolishes the MVB151 staining (Fig. 5*H*)]. This is very likely due to the fact that G93A aggregates sequester Hsp70, and without enough chaperone quality control substrates cannot be disaggregated and delivered to proteasomes. In fact, overexpressing Hsp70 blocked MVB151 staining of the toxic G93A JUNQs (Fig. 5*I*). These data suggest that, although toxic aggregates do not inhibit global proteasome function, they prevent quality control substrates in the JUNQ from being delivered to the proteasome. Additionally, these data provide rare evidence that proteasomal degradation takes place in aggregate inclusions.

Removing G93A from the JUNQ Rescues JUNQ Function. Because enhancing G93A aggregation reversed much of its toxic effect, we inquired whether this relocalization to the Htt inclusion also alleviated the underlying mechanistic causes of toxicity. Removing G93A from the JUNQ via the Htt-SOD1G93A fusion rescued the inhibition of VHL degradation by G93A (Fig. 5*C*). These findings provide evidence that aggregates can be either toxic or nontoxic depending on their subcellular localization, namely whether they are localized to an active JUNQ.

Insoluble Toxic Aggregates in JUNQ Cause Global Decline of Proteostasis. The data showing that toxic aggregates inhibit quality control function by exhausting quality control resources are consistent with the "proteostasis" model of aggregate toxicity (21). This model was put forth by a number of previous studies showing that accumulation of toxic aggregates results in the misfolding of marginally stable proteins. Accordingly, when we coexpressed one such protein, Luciferase, with G93A, we observed that it coaggregated with G93A in the JUNQ 100% of the time in all observed cells ($n = 50$), indicating a marked decline in proteostasis. After 12 h of expression, roughly one-half of the G93A-expressing cells showed aggregate inclusions. Luciferase never localized to the JUNQ when G93A was diffuse in the cytosol, and only rarely when Htt was coexpressed (Fig. 6*A*; cells with and without JUNQ inclusions exhibited the same levels of G93A and Luciferase fluorescence). Our study provides cell biological context for proteostasis impairment, namely that global misfolding may be caused by the localization of poorly soluble quality control substrates to the JUNQ and the resultant stress on the quality control system.

Overexpression of Hsp70 Rescues JUNQ Function and Cell Viability. Our results indicated that toxic aggregates interfere with the function of the JUNQ and sequester Hsp70. We therefore asked whether this effect could be reversed by overexpressing Hsp70. Hsp70 enhanced the mobility of VHL in the JUNQ, even in the presence of G93A (Fig. 6*B*), suggesting that some of the immobile VHL is liberated or refolded by Hsp70. We then

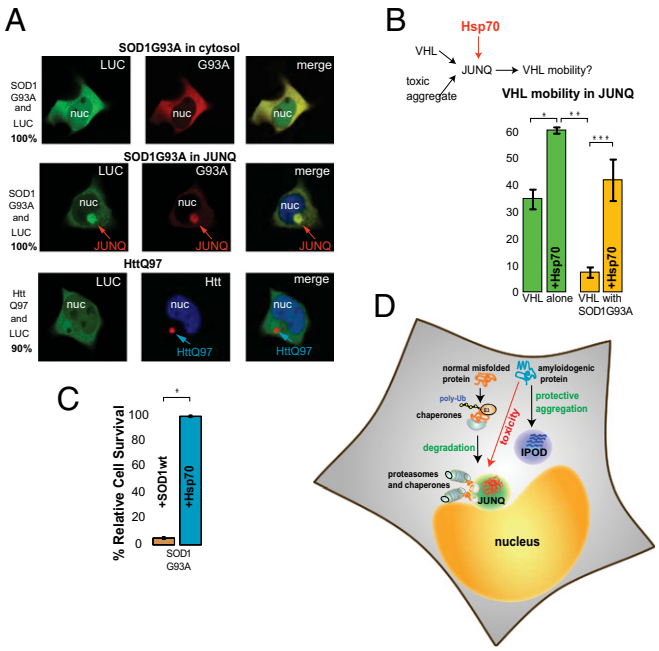

Fig. 6. Toxic proteins in the JUNQ impair proteostasis. (*A*) Luciferase accumulation in the JUNQ was observed only if G93A was there as well (*Center*), indicating that cells with G93A in the JUNQ have a decreased capacity to maintain proteostasis. Fifty cells coexpressing G93A and Luciferase were monitored for IBs. (*B*) Hsp70 enhances the solubility of VHL in the JUNQ. Hsp70 or empty vector were cotransfected with VHL and G93A. FRAP experiments were conducted as above. $*P \leq 0.0019$; $**P \leq 0.024$; $***P \leq 0.0044$. (*C*) Hsp70 reduces the toxic effects of G93A. G93A-CFP was cotransfected with either Hsp70-YFP or SOD1wt-YFP and sorted for YFP fluorescence, and cell viability was assessed as in Fig. 1*D*. $*P \leq 0.0004$. (*D*) Model for the relationship between toxicity and targeting to JUNQ or IPOD.

compared the effect of overexpressing Hsp70 (vs. SOD1WT as a control) on the viability of cells expressing G93A. Hsp70 significantly decreased G93A-induced toxicity (Fig. 6*C*). These data provide a mechanistic rationale for the long-standing observation that Hsp70 protects cells from aggregation toxicity in fly models (30) and mouse models of ALS (31). As we have shown, toxic aggregates inhibit the function of the JUNQ, and Hsp70 reverses this effect by increasing its quality control capabilities.

Discussion

The accumulation of proteins in aggregate inclusions has often been attributed to the decline of protein folding quality control during extreme stress or upon aging. Here, we assign quality control function to IBs, describing inclusion structures that promote toxicity, and others that help alleviate it. Hence, we suggest that inclusions are not always the result of a decline in quality control but may sometimes be the mediators of this decline.

We show that the JUNQ is a quality control compartment for soluble cytosolic misfolded proteins (Fig. 3). When the processing capacity of the JUNQ is overwhelmed, the result is a decrease in proteostasis (Figs. 5 and 6). This could explain the large number of proteins that have been shown to colocalize with disease-associated inclusions. Moreover, this type of model provides insight into the diversity of toxicity phenotypes observed in different disease models. For example, whereas in our systems (as well as in other cell and fly models) stress-induced Hsp70 seems to be the limiting factor that, when titrated, causes toxicity, in mouse models of ALS TDP43 (32) has been shown to colocalize with G93A inclusions (33). Hence, in different models of ALS the immediate cause of toxicity might be different, but the underlying decrease in proteostasis caused by inhibition of JUNQ function may be the initial trigger.

When toxic aggregates are prevented from localizing to the JUNQ, the result is a rescue of its quality control function and enhanced cell survival. In our emerging model, therefore, the JUNQ offers a method of sensing proteostasis stress, while insoluble inclusions enable the cell to benignly sustain high levels of aggregation. This model resolves a number of disparate studies in the field of aggregation, some suggesting that inclusion formation is toxic, and some showing that it is protective. We suggest that it is a basic cell biological phenomenon, which perhaps could be explored for designing disease intervention.

Our study reinforces a growing set of data showing that localization of aggregates in inclusions is an integral part of quality control, rather than the result of its breakdown (13, 17). Our data strongly suggest that aggregate inclusions, in addition to colocalizing with quality control components, are functional compartments. Other studies have also noted that active aggregation can be protective of cell viability, whereas solubilization of amyloidogenic proteins can actually lead to toxicity (11, 34, 35). The diverse susceptibility of different cell types to aggregate toxicity necessitates an exploration of the way all cells manage aggregates, in an effort to understand the differences between the general case, and the specific case of neurons afflicted in diseases. Hence, our study is focused on the way an individual nonneuronal cell experiences the toxicity associated with aggregation. Additionally, the formation of inclusions such as JUNQ, IPOD, ALIS, and others, is one stage of a multifactorial cellular process of aggregation quality control. Intermediate structures, such as cytosolic aggregate stress foci with no distinct localization, may also be relevant to understanding disease pathology, because aggregation intermediates may be trapped there in certain cell types (36).

Our findings establish a model for aggregation toxicity in which the toxicity of a protein aggregate is associated with its subcellular localization (Fig. 6*D*). In other words, where the aggregate is localized (JUNQ vs. other inclusions such as the IPOD, or stress foci in the cytosol) is likely just as important, if not more important, than which protein (Htt vs. SOD1) is aggregating. The data we have presented support the following model for progression of aggregate toxicity: first, poorly soluble quality control substrates are localized to the JUNQ where they sequester JUNQ-resident quality control factors. This results in the inhibition of quality control, leading to cell death. By identifying the cellular target of toxic aggregates, our study provides important insight into potential approaches for alleviating toxicity. The major challenge for future work will be to determine how triage between JUNQ, the cytosol, and other compartments is regulated in higher eukaryotes over the life span of the organism, and how the cell biological phenomena described here translate into animal models, especially during aging and disease. Aggregation disorders affect specific subtypes of cells (such as postmitotic neurons), with unique cell biology, gene expression patterns, and modes of quality control. In future studies, it will be essential to relate our findings pertaining to general cell biology, to the specific context of neuronal subtypes.

Materials and Methods

Imaging experiments were conducted with a Zeiss LSM710 microscope equipped with 488-, 406-, 561-, and 630-nm lasers. A 63× oil objective (N.A., 1.4) was used with 1% laser power. For live-cell experiments, a representative 1-μm-thick *Z* slice was taken. For some of the images, a Nikon A1R microscope was used with a 60× water objective (N.A., 1.27). Detailed Materials and Methods can be found in *SI Text*.

ACKNOWLEDGMENTS. We thank R. Morimoto, M. Brandeis, N. Dantuma, B. Florea, A. Kakizuka, H. Kampinga, A. Kisselev, S. Munro, H. Overkleeft, and M. Sherman for generous gifts of reagents; and M. Hecht, J. Goodhouse, and R. Sharivkin for technical assistance and advice. We also thank Jeremy England, Ehud Cohen, Michael Hecht, Mark Kaganovich, Maya Schuldiner, Hali Spokoini, and members of the D.K. laboratory for valuable discussion of the experiments and comments on the manuscript. This work was supported by Israel Science Foundation Grant 843/11 and a grant from the National Institute for Psychobiology in Israel.

1. Sherman MY, Goldberg AL (2001) Cellular defenses against unfolded proteins: A cell biologist thinks about neurodegenerative diseases. *Neuron* 29:15–32.
2. Gershenson A, Gierasch LM (2011) Protein folding in the cell: Challenges and progress. *Curr Opin Struct Biol* 21:32–41.
3. Hershko A, Ciechanover A (1998) The ubiquitin system. *Annu Rev Biochem* 67: 425–479.
4. Chiti F, Dobson CM (2006) Protein misfolding, functional amyloid, and human disease. *Annu Rev Biochem* 75:333–366.
5. Cohen E, Dillin A (2008) The insulin paradox: Aging, proteotoxicity and neurodegeneration. *Nat Rev Neurosci* 9:759–767.
6. McClellan AJ, Scott MD, Frydman J (2005) Folding and quality control of the VHL tumor suppressor proceed through distinct chaperone pathways. *Cell* 121: 739–748.
7. Aguzzi A, Calella AM (2009) Prions: protein aggregation and infectious diseases. *Physiol Rev* 89:1105–1152.
8. Matsumoto G, Stojanovic A, Holmberg CI, Kim S, Morimoto RI (2005) Structural properties and neuronal toxicity of amyotrophic lateral sclerosis-associated Cu/Zn superoxide dismutase 1 aggregates. *J Cell Biol* 171:75–85.
9. Bosco DA, LaVoie MJ, Petsko GA, Ringe D (2011) Proteostasis and movement disorders: Parkinson's disease and amyotrophic lateral sclerosis. *Cold Spring Harb Perspect Biol* 3:a007500.
10. Arrasate M, Mitra S, Schweitzer ES, Segal MR, Finkbeiner S (2004) Inclusion body formation reduces levels of mutant huntingtin and the risk of neuronal death. *Nature* 431:805–810.
11. Cohen E, Bieschke J, Perciavalle RM, Kelly JW, Dillin A (2006) Opposing activities protect against age-onset proteotoxicity. *Science* 313:1604–1610.
12. Nilsberth C, et al. (2001) The "Arctic" APP mutation (E693G) causes Alzheimer's disease by enhanced Abeta protofibril formation. *Nat Neurosci* 4:887–893.
13. Treusch S, Cyr DM, Lindquist S (2009) Amyloid deposits: Protection against toxic protein species? *Cell Cycle* 8:1668–1674.
14. Shorter J, Lindquist S (2004) Hsp104 catalyzes formation and elimination of self-replicating Sup35 prion conformers. *Science* 304:1793–1797.
15. Kaganovich D, Kopito R, Frydman J (2008) Misfolded proteins partition between two distinct quality control compartments. *Nature* 454:1088–1095.
16. Kopito RR (2000) Aggresomes, inclusion bodies and protein aggregation. *Trends Cell Biol* 10:524–530.
17. Tyedmers J, Mogk A, Bukau B (2010) Cellular strategies for controlling protein aggregation. *Nat Rev Mol Cell Biol* 11:777–788.
18. Zhang X, Qian S-B (2011) Chaperone-mediated hierarchical control in targeting misfolded proteins to aggresomes. *Mol Biol Cell* 22:3277–3288.
19. Matsumoto G, Kim S, Morimoto RI (2006) Huntingtin and mutant SOD1 form aggregate structures with distinct molecular properties in human cells. *J Biol Chem* 281: 4477–4485.
20. Zaarur N, Meriin AB, Gabai VL, Sherman MY (2008) Triggering aggresome formation: Dissecting aggresome-targeting and aggregation signals in synphilin 1. *J Biol Chem* 283:27575–27584.
21. Morimoto RI (2008) Proteotoxic stress and inducible chaperone networks in neurodegenerative disease and aging. *Genes Dev* 22:1427–1438.
22. Rujano MA, et al. (2006) Polarised asymmetric inheritance of accumulated protein damage in higher eukaryotes. *PLoS Biol* 4:e417.
23. Wang J, et al. (2009) An ALS-linked mutant SOD1 produces a locomotor defect associated with aggregation and synaptic dysfunction when expressed in neurons of *C. elegans*. *PLoS Genet* 5:e1000350.
24. England JL, Kaganovich D (2011) Polyglutamine shows a urea-like affinity for unfolded cytosolic protein. *FEBS Lett* 585:381–384.
25. Kobayashi T, Tanaka K, Inoue K, Kakizuka A (2002) Functional ATPase activity of p97/VCP is required for the quality control of ER in neuronally differentiated mammalian PC12 cells. *J Biol Chem* 277:47358–47365.
26. Hayward LJ, et al. (2002) Decreased metallation and activity in subsets of mutant superoxide dismutases associated with fALS. *J Biol Chem* 277:15923–15931.
27. McClellan AJ, Tam S, Kaganovich D, Frydman J (2005) Protein quality control: Chaperones culling corrupt conformations. *Nat Cell Biol* 7:736–741.
28. Menéndez-Benito V, Heessen S, Dantuma NP (2005) Monitoring of ubiquitin-dependent proteolysis with green fluorescent protein substrates. *Methods Enzymol* 399:490–511.
29. Verdoes M, et al. (2006) A fluorescent broad-spectrum proteasome inhibitor for labeling proteasomes in vitro and in vivo. *Chem Biol* 13:1217–1226.
30. Warrick JM, et al. (1999) Suppression of polyglutamine-mediated neurodegeneration in *Drosophila* by the molecular chaperone HSP70. *Nat Genet* 23:425–428.
31. Gifondorwa DJ, et al. (2007) Exogenous delivery of heat shock protein 70 increases lifespan in a mouse model of amyotrophic lateral sclerosis. *J Neurosci* 27:13173–13180.
32. King OD, Gitler AD, Shorter J (2012) The tip of the iceberg: RNA-binding proteins with prion-like domains in neurodegenerative disease. *Brain Res* 1462:61–80.
33. Shan X, Vocadlo D, Krieger C (2009) Mislocalization of TDP-43 in the G93A mutant SOD1 transgenic mouse model of ALS. *Neurosci Lett* 458:70–74.
34. Subramaniam S, Snyder SH (2011) Huntington's disease is a disorder of the corpus striatum: focus on Rhes (Ras homologue enriched in the striatum). *Neuropharmacology* 60:1187–1192.
35. Douglas PM, et al. (2008) Chaperone-dependent amyloid assembly protects cells from prion toxicity. *Proc Natl Acad Sci USA* 105:7206–7211.
36. Herrera F, Outeiro TF (2012) α-Synuclein modifies huntingtin aggregation in living cells. *FEBS Lett* 586:7–12.

Supporting Information

Weisberg et al. 10.1073/pnas.1205829109

SI Materials and Methods

Confocal Microscopy. Imaging and fluorescence recovery after photobleaching (FRAP) experiments were conducted with a Zeiss LSM 710 laser-scanning microscope equipped with a 20-mW tunable 488-nm argon ion laser, and solid-state 406-, 561-, and 630-nm lasers. A 63× apochromat oil-objective (N.A., 1.4) was used with 1% laser power, except for FRAP images. Images were acquired with alternating line scans, except for FRAP in which images were acquired with a single scan. Images were processed with Zeiss LSM Image Browser software. For most live-cell experiments, a representative 1-μm-thick Z slice was taken. For some of the images, a Nikon A1R laser-scanning confocal microscope was used with a 60× apochromat water objective (N.A., 1.27), with identical experimental setting as for the Zeiss. Fifty cells per visual phenotype were examined to determine the percentage of localization phenotype, indicated to the left of the images.

MTS Cell Survival Assay. Cells were seeded on a 10-cm plate and transfected with 0.5 μg of empty pSLIK vector and 2.5 μg of SOD1G93A-YFP, SOD1wt-YFP, HttQ97-SOD1G93A-YFP, HttQ97-mRFP, or VHL-GFP. Eighteen hours after transfection, cells were sorted based on equal levels of fluorescence. Cells were seeded in a 96-well plate at 10,000 cells per well and allowed to recover and divide for 7 d. On days 3, 5, and 7 after sorting, cell proliferation was measured using the CellTiter 96 AQueous One Solution Cell Proliferation Assay (Promega), as per the manufacturer's instructions. Measurements were done in triplicate. Background absorbance was subtracted from the reading, and values were normalized to the nontoxic SOD1wt-YFP. Data shown are from day 7 reading. For Hsp70 coexpression rescue assay, cells were transfected with 0.5 μg of empty pSLIK vector, 2.5 μg of SOD1G93A-CFP, and 2.5 μg of Hsp70-YFP or SOD1wt-YFP.

Proteasome Occupancy Assay. Cells were grown to 50–70% confluence in eight-well tissue culture slides (ibiTreat; #80826; ibidi GmBh) and transfected with 0.5 μg of SOD1G93A-CFP with or without 1 μg of pcDNA3.1-Hsp70-GFP, or with 1 μg of pcDNA3.1-VHL-GFP. Thirty-six hours after transfection, cells were stained with 500 nM BODIPY-TMR–MVB151 (1) for 1 h. Cells co-incubated with MG132 were used as negative control. Cells were washed with DMEM without Phenol Red (Gibco; #31053028), and pictures were acquired with Nikon A1R confocal microscope equipped with 37 °C humidified incubator as described above).

Mammalian Cell Culture. HEK 293 cells were maintained in DMEM (Gibco) supplemented with 50 mL/500 mL FBS, 100 units/mL penicillin, 0.1 mg/mL streptomycin at 37 °C in an atmosphere of 5% CO_2, 95% air. For imaging and FRAP experiments, cells were plated on poly-L-lysine (Sigma)-coated glass bottom plates (MatTek). Stable cell lines were generated by selecting with 1 mg/mL G418 (Gibco) and maintained in 0.7 mg/mL G418.

Plasmids and Transfections. Unless otherwise noted, all transfections were done using jet-PEI (PolyPlus Transfection) according to manufacturer's instructions. Medium containing PEI and DNA was washed out 8 h posttransfection. pTRE plasmids were co-transfected with empty pSLIK vector. When necessary, expression was induced with 1 μg/mL doxycycline (Sigma). pcDNA3.1-VHL-GFP, pcDNA3.1-mCherry-VHL, pcDNA3.1-HttQ97-mRFP2.1 plasmids were as described in ref. 2. pTRE-SOD1G93A-YFP, pTRE-SOD1G93A-CFP, pTRE-SOD1wt-YFP, pEYFP-N1-LMP2, and pEYFP-N1-HSP70 plasmids were a gift from Richard Morimoto (Northwestern University, Evanston, IL), pEYFP-N2-Cyt-Luciferase plasmid was a gift from Harm Kampinga (University of Groningen, Groningen, The Netherlands), mCherry- and GFP-Ubiquitin were a gift from Michael Brandeis (Hebrew University, Jerusalem, Israel), RFP-pericentrin was a gift from Sean Munro, and pEYFP-N3-VCPwt was a gift from Akira Kakizuka (Kyoto University, Kyoto, Japan). Ub-R-YFP constructs were purchased from Addgene. pTRE-HttQ97-SOD1-G93A-YFP and pTRE-HttQ97-SOD1G93A-CFP were generated by subcloning the PCR-amplified HttQ97 fragment into the pTRE-SOD1G93A-YFP or pTRE-SOD1G93A-CFP constructs.

FRAP. A region of interest corresponding to 15% of the inclusion area was bleached using either a 488-nm laser for 2 s at full laser power, and single scan images were collected every 1 s for 5 min following the bleach. Fluorescence of the bleached region of interest (F) was calculated as $F = (I_i - I_b)/(I_r - I_b)$, where I_i is fluorescence intensity in the region of interest, I_r is intensity in a reference area (either at some distance in the same cell or in another cell), and I_b is background intensity (outside all cells). Intensity data were recorded using Zeiss Zen software. Mobile fraction (M_f) was calculated as $M_f = (F_f - F_0)/(F_i - F_0)$, where F_f is fluorescence after full recovery, F_0 is fluorescence immediately after the bleach, and F_i is fluorescence before bleaching (3). Reported M_f values are the average of 10 data points. For fluorescence loss in photobleaching experiments, a 2 × 2 μm area of the cytosol was bleached continuously (with each scan), while the fluorescence of the inclusion and a control cytosolic region close to the inclusion were measured.

Whole Lysate VHL Solubility Assay. Cells were seeded on a 10-cm plate and transfected with 0.5 μg of empty pSLIK vector, 2.5 μg of VHL-GFP, and 2.5 μg of SOD1G93A-YFP, SOD1wt-YFP, HttQ97-mRFP, or empty vector. Forty-eight hours posttransfection, cells were lysed in 100 μl of ice-cold Triton-DOC lysis buffer (0.5% Triton X-100, 0.46% Na-deoxycholate, 150 mM NaCl, 10 mM Tris·HCl, pH 7.5, 10 mM EDTA). Lysates were immediately centrifuged 3,000 × g for 5 min at RT in an Eppendorf microfuge. Biochemical analyses were performed on the postnuclear supernatant (PNS). Aggregated proteins were separated from soluble fractions by sedimentation: PNS were brought to 1% Sarkosyl, incubated on ice for 30 min, and then spun at 100,000 × g for 1 h at 4 °C in a TLA120.2 rotor. The pellets were then resuspended in lysis buffer. Samples were boiled in SDS loading buffer and then subjected to SDS/PAGE electrophoresis and immunoblotting with an anti-GFP-HRP-conjugated antibody (Invitrogen). Protein concentration was quantified before resolving by gel instead of using a loading control, which is not possible for a sup-pellet assay. Signal was visualized using a Bio-Rad ChemiDoc XRS+ scanner and quantified using ImageLab3.0.1 software.

Immunohistochemistry Experiments. The ALS patient and control spinal cord sections were obtained from the Center for Neurodegenerative Disease Research at the University of Pennsylvania. Sections were deparaffinized before pretreatment using heat antigen retrieval with Bull's Eye Decloaker (BioCare Medical). After washing with 0.1% PBST and blocking with 10% goat serum, 0.5% PBST for 30–60 min at 25 °C, sections were incubated with mouse anti-SOD1 (1:50; Sigma), mouse anti-alpha7

(1:50; Enzo Life Sciences), mouse anti-VCP/p97 (1:50; Abcam), mouse anti-ubiquitin (1:50; Assay Designs), or rabbit anti-Hsp70 (1:50; Assay Designs) in 0.1% PBST overnight at 4 °C. After washing with 0.1% PBST, sections were incubated with Alexa Fluor 488- or 594-conjugated goat anti-mouse or rabbit IgG (1:200; Vector Laboratories) for 1 h at 25 °C. In pilot studies to work out antibody staining conditions, we performed "no primary antibody" controls. Also, for the single antibody-stained sections, we visualized staining in both the Alexa 488 and 594 channels and confirmed that we only detected fluorescence in the appropriate channel for the given secondary antibody. Both of these control experiments allowed us to distinguish SOD1+ inclusions from autofluorescence from lipofuscin. Detailed immunohistochemistry protocols are available at http://www.med.upenn.edu/mcrc/.

***P* Values for Data Shown in Fig. 2.** P(SOD1wt vs. G93A) ≤ 0.0046; P(SOD1wt vs. Htt) ≤ 0.0297; P(SOD1wt vs. Htt-SOD1G93A) ≤ 0.0595; P(VHL vs. G93A) ≤ 0.0001; P(VHL vs. Htt) ≤ 0.003; P(VHL vs. Htt-SOD1G93A) ≤ 0.0006; P(G93A vs. HttQ97) ≤ 0.0695; P(G93A vs. Htt-SOD1G93A) ≤ 0.0005 (Student's t test).

1. Verdoes M, et al. (2006) A fluorescent broad-spectrum proteasome inhibitor for labeling proteasomes in vitro and in vivo. *Chem Biol* 13:1217–1226.
2. Kaganovich D, Kopito R, Frydman J (2008) Misfolded proteins partition between two distinct quality control compartments. *Nature* 454:1088–1095.
3. Shan X, Vocadlo D, Krieger C (2009) Mislocalization of TDP-43 in the G93A mutant SOD1 transgenic mouse model of ALS. *Neurosci Lett* 458:70–74.

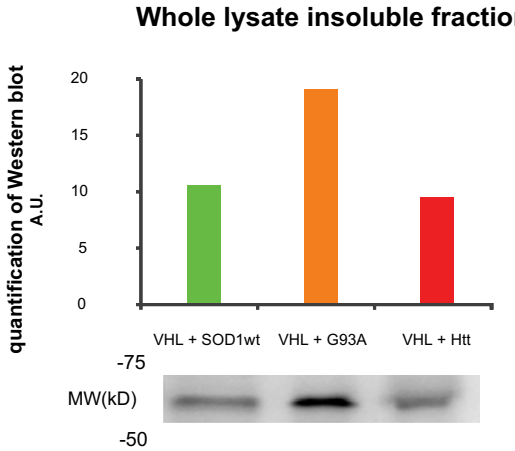

Fig. S1. (*A*) Quantification of biochemical analysis of VHL-GFP solubility in different conditions validates FRAP results. Sedimentation analysis was conducted with Sarkosyl buffer, as described in *SI Materials and Methods*. Coexpression of SOD1G93A-CFP, but not HttQ97-mRFP, increased the fraction of VHL-GFP in the pellet after centrifugation.

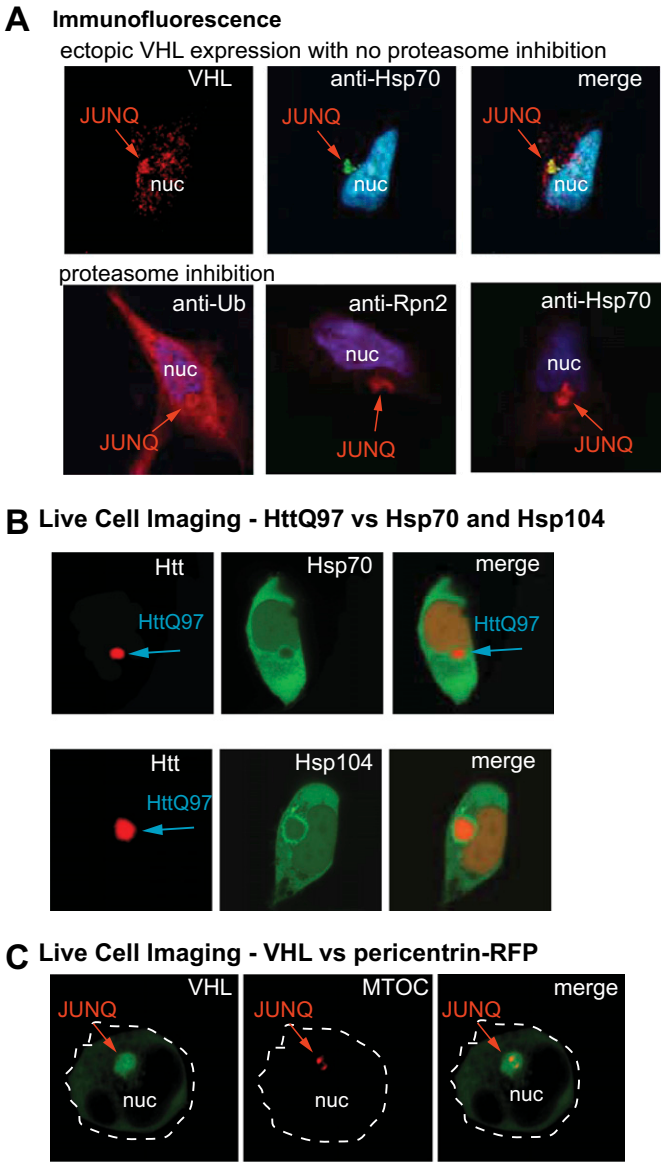

Fig. S2. (*A*) Endogenous quality control factors localize to the JUNQ. Cells ectopically overexpressing VHL-GFP (*Upper*) or treated with proteasome inhibitor (2 μM MG132 for 6 h) (*Lower*) showed enhanced staining for Hsp70, 19S proteasomes, and ubiquitinated proteins in a juxtanuclear location. (*B*) Hsp70-YFP does not colocalize with the HttQ97 inclusion (*Upper*). Hsp104-GFP, an amyloid-binding chaperone and an IPOD marker colocalizes with the HttQ97-mRFP inclusion (*Lower*). (*C*) VHL-GFP in a representative JUNQ inclusion colocalizes with the MTOC labeled by RFP-pericentrin in live cells.